Volume 3
Number 4
April 2024
Pages 481–710

Sensors & Diagnostics

rsc.li/sensors

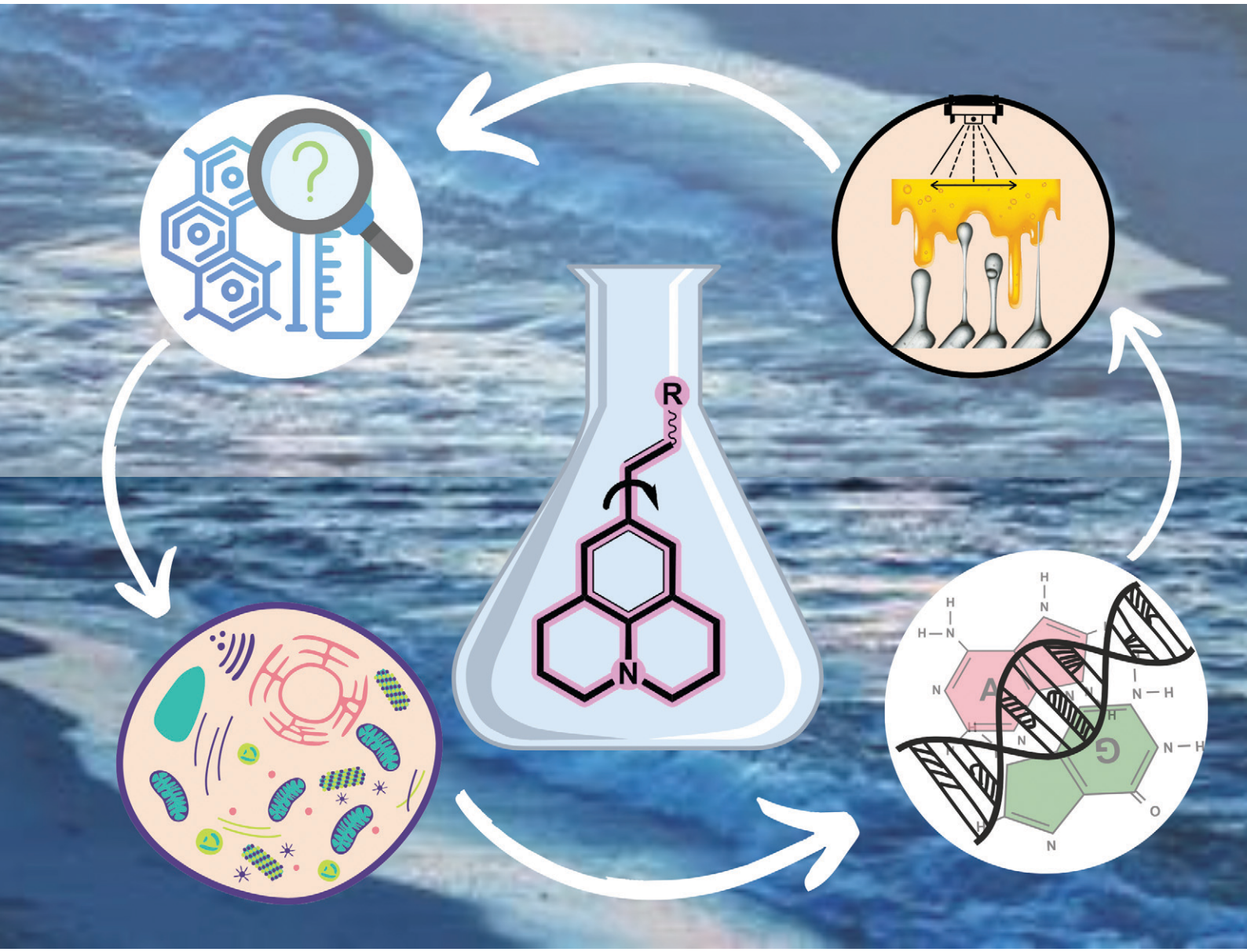

ISSN 2635-0998

ROYAL SOCIETY OF CHEMISTRY

TUTORIAL REVIEW
Apurba Lal Koner *et al.*
Julolidine-based fluorescent molecular rotor: a versatile tool for sensing and diagnosis

Sensors & Diagnostics

TUTORIAL REVIEW

View Article Online
View Journal | View Issue

Cite this: *Sens. Diagn.*, 2024, **3**, 585

Julolidine-based fluorescent molecular rotor: a versatile tool for sensing and diagnosis

Nabashree Chakraborty,† Akshay Silswal † and Apurba Lal Koner *

Fluorescent molecular rotors incorporating julolidine have found diverse applications in various fields. Recently, researchers have explored their utility in polymerization, metal ion detection, self-assembly, aggregation, and detection of proteins and nucleic acids. These julolidine-based molecular rotors primarily serve as fluorescent turn-on probes, showcasing their effectiveness in sensing local environmental properties such as polarity, pH, viscosity, protein folding, and misfolding. This comprehensive review covers an array of julolidine-based fluorescent molecular rotors, along with their pertinent uses in the field of biological research and monitoring changes in the microenvironment through solvent dielectric constant, viscosity, self-assembled polymers, and submicrometer-sized membrane-bound compartments in live cellular systems. The discourse supports ongoing research concerning their diverse applications and provides a forward-looking perspective on their potential advancements.

Received 16th December 2023,
Accepted 20th February 2024

DOI: 10.1039/d3sd00334e

rsc.li/sensors

1. Introduction

Fluorescence spectroscopy and analysis technology have advanced significantly in the 20th and 21st centuries, leading to discoveries of numerous fluorescent dyes and instrumentation advancements. Over the years, fluorescence-based methods and time-resolved fluorescence have been employed as tools for sensing, and their employment in sensing microenvironments has dramatically increased.[1–4] Numerous strategies have emerged for sensing involving phenomena like intramolecular charge transfer (ICT), photoinduced electron transfer (PET), Förster/fluorescence resonance energy transfer (FRET), twisted intramolecular charge transfer (TICT), excited-state intramolecular proton transfer (ESIPT) and others.[5–9] Based on these phenomena, fluorescence-based microscopy techniques are commonly employed to monitor important factors such as viscosity, polarity, pH, temperature, and hypoxia in microenvironments.[10] These factors play a crucial role in biological processes. Cellular imaging using small fluorescent molecules is a prevalent approach to understanding the dynamics and characterization of bioanalytes as well as various biological processes. Fluorescent molecular rotors (FMRs) are a class of molecules that have emerged as tools for sensing owing to their high signal-to-noise ratio properties.[11–13] Fluorescence imaging techniques based on FMRs are non-invasive and

Bionanotechnology Lab, Department of Chemistry, Indian Institute of Science Education and Research Bhopal, Bhopal Bypass Road, Bhauri, Bhopal-462066, Madhya Pradesh, India. E-mail: akoner@iiserb.ac.in
† Contributed equally to this work.

Nabashree Chakraborty

Ms. Nabashree Chakraborty completed her Master's degree in Chemistry from Central University of Karnataka, India. Currently, she is working as a PhD scholar at Dr. Apurba Lal Koner's lab in IISER Bhopal. She is involved in research related to the synthesis of fluorescent molecules and their spectroscopic investigations.

Akshay Silswal

Dr. Akshay Silswal obtained his doctoral degree in Chemistry from IISER Bhopal. During his doctoral research, he was involved in developing fluorescent molecular rotors for targeting specific cellular organelles to understand their biophysical properties. His current research is centered on advancing fluorophores and utilizing them for sensing and photocatalysis applications.

provide quick, real-time, and spatiotemporal information about the microenvironment.[2] Over the years, researchers have developed various kinds of molecular rotors for monitoring alteration in the proteins, polymers, and cellular environment. Ongoing research is focused on developing molecular rotors that emit light in the far-red or near-infrared region, aiming for practical applications in real-world scenarios.

The FMR is a type of molecule that can experience intramolecular rotation when exposed to light. If this rotation is unrestricted, the molecules will return to their ground state from an excited state through non-radiative pathways. However, if the rotation is limited by factors such as the viscosity of the surrounding environment, the molecules will exhibit increased fluorescence. Molecular rotors encompass a diverse class of molecules that exhibit non-radiative decay mechanisms beyond TICT. These rotors typically consist of a fluorophore attached to a conjugated moiety capable of rotational motion relative to the entire molecule (Fig. 1). Moreover, some molecular rotors leverage this rotational motion to induce dimer emission, contributing to their distinct classification within this category. The class of FMRs consists of three subunits: an electron donor, an electron acceptor, and an electron-rich conjugated linker that has alternating single and double bonds, and will be discussed here. Upon photoexcitation, these molecules undergo a TICT state, which has a lower energy in the excited state. This twisting facilitates intramolecular charge transfer between the donor and acceptor, resulting in the creation of a charge-separated state as electrons transfer from the donor to the acceptor. This charge separation is highly polar and is significantly stabilized by polar solvents. The relaxation of the molecule from this state can lead to either red-shifted emission or non-radiative relaxation, depending on the molecular structure. Incorporating certain parameters enhances the TICT effect. These parameters include increasing the electron donor strength, initial twisting of the molecule, increasing the electron acceptor strength, and engineering the bridge. Manipulating these factors allows for tuning the TICT phenomenon. In this review, we discuss julolidine-based molecular rotors and their diverse applications since 2014.

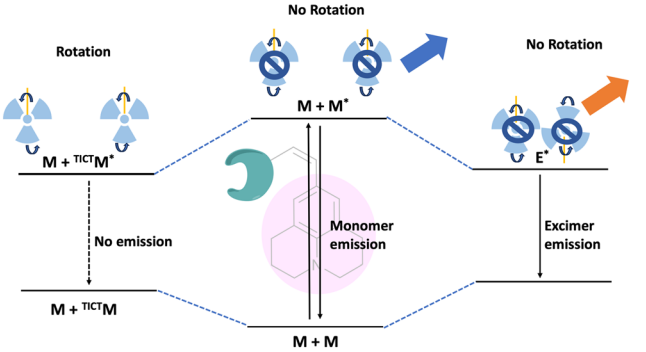

Fig. 1 Modified Jablonski diagram for understanding the fluorogenic response in julolidine-based FMRs, M: monomer, ^{TICT}M: monomer in the twisted intramolecular charge transfer state M*: excited monomer, ^{TICT}M*: excited monomer in the twisted intramolecular charge transfer state, and E*: excimer.

The molecule 9-(dicyanovinyl)-julolidine (**DCVJ**) is widely known for its fluorescence properties that are dependent on viscosity. Prof. Theodorakis and co-workers have extensively worked with 9-(2-carboxy-2-cyanovinyl) julolidine (**CCVJ**) and **DCVJ**-based molecular rotors for various applications.[14–18] They are commonly used for measuring viscosity in cell membranes of liposomes, monitoring polymerization processes, and tubulin remodeling. However, when using **DCVJ** for measuring membrane viscosity, there are often challenges, such as poor water solubility and a tendency to bind serum proteins. This can result in protein-bound **DCVJ** leaking into the cytoplasm and causing a background signal. To address this issue, Haidekker *et al.* modified the nitrile group of **DCVJ** with esters containing different alkyl chains. This alkyl substitution improved the localization of the molecule in the membrane. The probe with farnesyl substitution (farnesyl-(2-carboxy-2-cyanovinyl)-julolidine, **FCVJ**) exhibited better viscosity-sensitive properties and improved photostability compared to **DCVJ**. Additionally, the research group developed a ratiometric fluorescence approach to quantify viscosity. They combined the polarity-insensitive **CMAM** (2-cyano-3-(4dimethylaminophenyl) acrylic acid methyl ester) with the polarity-sensitive **MCCA** (7-methoxycoumarin-3-carboxylic acid) to create a ratiometric fluorescence response. In this approach, **CMAM** acts as a donor to excite **MCCA**, which serves as a sensor for viscosity through resonance energy transfer. The fluorescence intensity of **CMAM** remains constant and acts as a reference, while **MCCA** changes in response to viscosity variations. A normalized intensity is obtained by dividing the emission intensity of the sensor by the emission intensity of the reference. This eliminates concentration-related effects and provides a method for quantifying viscosity using an internal reference. Recently, julolidine-based molecular rotors have been utilized for various applications which are discussed in detail.

Apurba Lal Koner

Dr. Apurba Lal Koner is an Associate Professor at the Department of Chemistry in IISER Bhopal. One of his current research interests lies in the design and synthesis of novel fluorescent reporters for live-cell fluorescence imaging for understanding sub-cellular properties.

2. Applications of julolidine-based FMRs

2.1 Sensing of proteins and DNA

In 2014, Goh and co-workers explored the binding of the molecular rotor, **CCVJ**, to streptavidin by conjugating it to biotin.[19] They observed a two-fold increase in fluorescence upon the addition of streptavidin, indicating the effectiveness of the biotin-rotor probe. In their model system they focused on the interaction between Mdm2 and p53, which is clinically relevant and a significant target in drug discovery. They conjugated the **CCVJ** rotor to two peptides, **JP1** and **JP2**, derived from a phage display screen. Despite only differing by a single amino acid, **JP1** and **JP2** exhibited a ten-fold difference in binding affinities. When the JP1–rotor conjugate (**JP1–R**) was co-incubated with Mdm2 protein, they observed a concentration-dependent increase in fluorescence activity (Fig. 2a).

The fluorescence signal previously observed in the **JP1–R**–Mdm2 complex was completely eliminated when racemic Nutlin was added, likely due to the displacement of **JP1–R** from Mdm2. In contrast, the addition of Mdm2 did not cause any significant changes in fluorescence intensity in **JP2–R**. During the interaction with nonspecific proteins eIF4E, BSA, and IgG, the addition of **JP1–R** did not result in any fluorescence increase (Fig. 2b) across the same concentration range for all three proteins. The presence of nonspecific proteins led to low levels of rotor activity, indicating potential applicability in complex biological samples. Molecular dynamics simulations suggest that the C-terminal end of **JP1–R** adopts a helical turn, influenced by the hydrogen bonds between the hydroxyl side chain and backbone of S12, as well as the backbone carbonyl of W8.

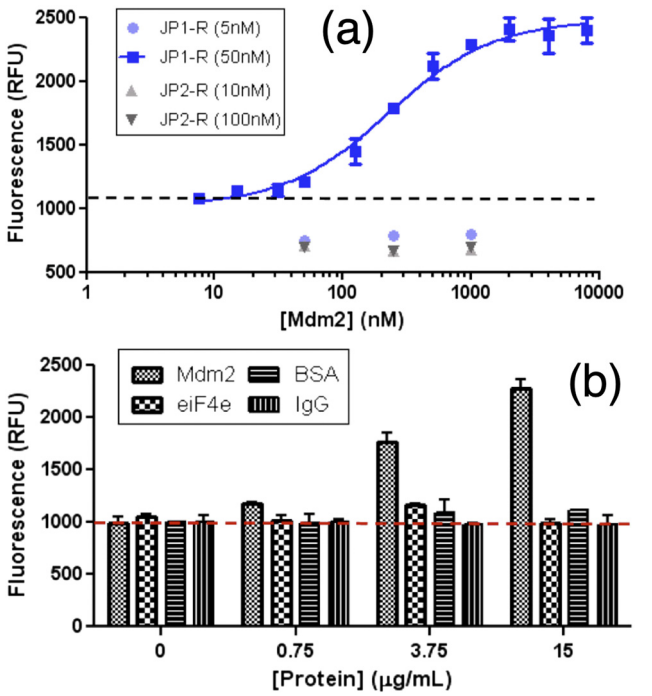

Fig. 2 Increasing fluorescence of **JP1–R** when bound specifically to recombinant Mdm2. (a) Higher Mdm2 concentrations were then added to stable concentrations of rotary–peptide conjugates (**JP1–R**, **JP2–R**). (b) **JP1–R** added to increasing Mdm2 (18–125 residues) EIF4e BSA IGG 50 nM JP1–R; dashed-line indicates background fluorescence only. Reprinted with permission from ref. 19. Copyright 2014. American Chemical Society.

The apparent K_d for Mdm2 binding was determined to be 16.01 ± 7.52 nM based on the **JP1–R** fluorescence measurements. This value correlates well with the previously reported K_d of 18.83 ± 5.03 nM obtained using isothermal titration calorimetry (ITC). In order to further confirm the binding of **JP1–R**, we conducted ITC experiments and obtained a K_d of 10.2 ± 7.97 nM, which is consistent with the fluorescence-based measurement. On the other hand, the calculated apparent K_d for **JP2–R** was found to be 3365 ± 640.6 nM, which is approximately 14-fold lower than the previously reported value of 239.81 ± 53.79 nM. The molecular rotor's TICT property is utilized to decrease its free volume when it interacts with a protein. This straightforward fluorescence turn-on signal, triggered by protein binding, enables the creation of sensitive and easy assays to measure protein–ligand binding in a high-throughput manner.

In 2015, Gavvala and his co-workers aimed to examine the fluorescence properties of **CCVJ** in different environments, such as cyclodextrins (CDs) and human serum albumin (HSA), using the femtosecond fluorescence up-conversion technique.[20] The absorption maximum of **CCVJ** experiences a blue shift in the presence of HSA (Fig. 3a), suggesting that **CCVJ** binds to HSA. A significant enhancement accompanied with a blue shift in the emission intensity of **CCVJ** was observed upon HSA binding (Fig. 3b). The calculated binding constant (K_a) between **CCVJ** and HSA is 1.0×10^5 M^{-1}, indicating a high affinity for binding. The binding of **CCVJ** with HSA is supported by electrostatic and hydrogen bonding interactions, as the negatively charged *E* isomer of **CCVJ** is surrounded by positively charged basic amino acid residues. Based on the findings presented in this paper, it can be inferred that the photo-isomerization process, known as the primary non-radiative decay pathway of **CCVJ**, is significantly limited within the aforementioned bio-mimetic and biological nano-cavities. Theoretical and molecular modeling studies have explored the potential orientations of **CCVJ** within the nano-cavities of CDs and proteins.

The Mukhopadhyay group utilized a **DCVJ** probe for monitoring the oligomerization of human β_2 microglobulin (β_2m).[21] The **DCVJ** probe binds to early amyloidogenic oligomers and is employed to examine the oligomerization of β_2m under varying NaCl concentration at pH 2.5. Additionally, the researchers used **DCVJ** to observe the rapid formation of early oligomers on the submillisecond time scale employing a stopped-flow mixing device for this purpose.

Lapidus and colleagues utilized **DCVJ** for detecting the oligomerization of amyloids.[22] The introduction of Aβ40 had no discernible impact on the **DCVJ** fluorescence over a 20-minute period. This could be attributed to either the non-

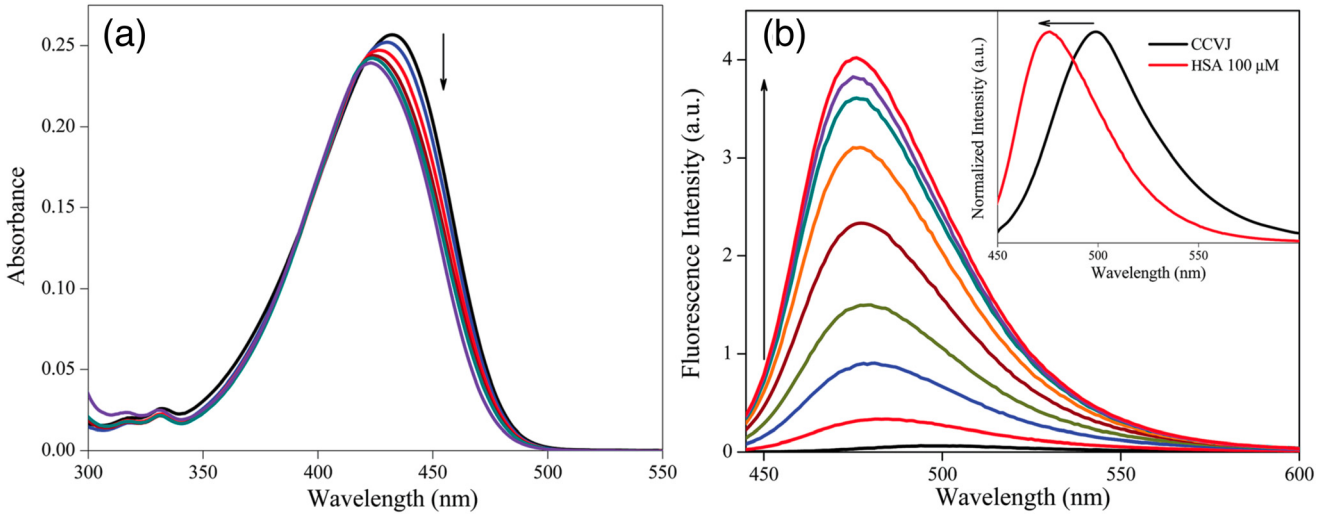

Fig. 3 Change in (a) absorption and (b) emission spectra of **CCVJ** with increasing concentration of HSA. Inset shows the normalized spectra of only **CCVJ** and with 10 μM HSA. Reprinted from ref. 20. Copyright 2015. Royal Society of Chemistry.

binding of **DCVJ** to the monomer or the high flexibility of the chain, which did not impede the rotation of bound **DCVJ**. The ability of **DCVJ** to discern oligomer structure and packing makes it a suitable probe for detecting the early lag phase of amyloid assembly.

Fares and his co-workers combined a fluorescent molecular rotor **CCVJ** with a mutated protein domain called AgHalo.[23] In non-stressed cells, the sensor remains folded and non-fluorescent. However, when exposed to stress conditions, it becomes fluorescent. This sensor is unique in its ability to detect misfolded proteins that cannot be detected by other existing sensors. This misfolding causes exposure of nonpolar and aromatic residues to a hydrophilic environment. The misfolded proteins are often associated with various diseases. Early detection of misfolded proteins and monitoring their aggregation can provide valuable insights into the progression of diseases and help in the development of therapeutic strategies.

The behavior of the Halo-tag with P1 and P2 ligands is different. P1 is a solvatochromic fluorophore that detects exposed hydrophobic regions of misfolded proteins. It can specifically detect AgHalo in conformations such as soluble oligomers and insoluble aggregates in live cells. However, P1 cannot detect AgHalo monomers that adopt misfolded conformations in cells. P2 is a fluorescent molecular rotor that detects protein aggregation by hindering the rotation of the rotor. When P2 is conjugated to AgHalo, it can detect the formation of misfolded conformations induced by proteome stress. P2 exhibits a higher fluorescence signal when detecting soluble and insoluble protein aggregates induced

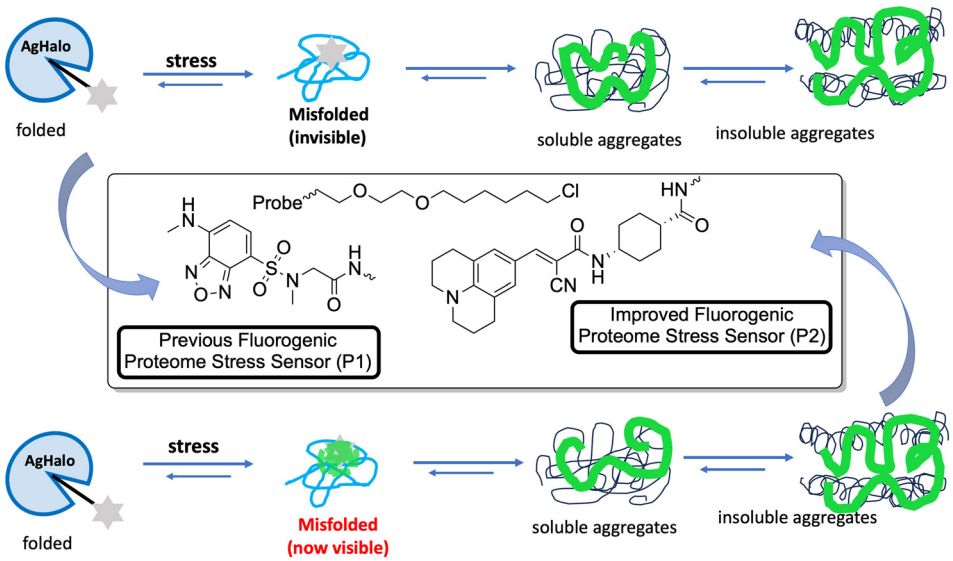

Fig. 4 Fluorogenic probes for the AgHalo sensor for understanding protein aggregation.

by more severe proteome stress. P1 detects exposed hydrophobic regions of misfolded proteins, while P2 detects protein aggregation by hindering the rotation of the fluorescent molecular rotor (Fig. 4).

At the end there are few limitations of this study. While the new sensor is more sensitive to misfolded conformations induced by mild proteome stress compared to previous sensors, it may still have limitations in detecting subtle changes in protein conformation. The sensor is designed to detect protein misfolding and aggregation, but it may not be able to distinguish between different types of protein aggregates or accurately identify specific misfolded proteins. The sensor's performance may vary in different cell types or under different cellular conditions, which could affect its ability to accurately detect proteostasis deficiency. The presence of other cellular components or molecules could potentially interfere with the sensor's fluorescence signal, leading to false-positive or false-negative results. While the sensor has been demonstrated in live cells, its applicability in more complex biological systems, such as animal models or human tissues, remains to be explored.

Recently to overcome the aforementioned challenges, Liu and co-workers have reported a dual-color fluorogenic thermal shift assay to measure changes in the melting temperatures of the protein system *via* bioorthogonal labeling.[24] In this assay, CCVJ functions as a fluorescent reporter by conjugating using sortase-tag technology to the target protein. This makes it possible to use two orthogonal fluorescence readouts for simultaneous monitoring of the aggregation of two distinct proteins and for orthogonal detection. CCVJ and another fluorescent rotor *i.e.*, Mero, were utilized for the multi-color detection of protein aggregates with minimal fluorescence cross-talk. The study provided a quantitative analysis on the thermodynamic interplay during protein co-aggregation.

The application of a structurally different molecular rotor in SNAP tag technology was also utilized to visualize intracellular compartments of cells and protein aggregates. Mostly, a 4-hydroxybenzylidene imidazolinone (HBI)-based molecular rotor was appended with O^6-benzyl-guanine (BG) for tagging with SNAP protein to achieve a fluorogenic response.[25–27]

Nath and his colleagues explored the interaction between the molecular rotor **DCVJ** and DNA.[28] **DCVJ**, a neutral molecule, exhibits a significant binding affinity to DNA, primarily attributed to ion–dipole interactions arising from its substantial dipole moment in the ground electronic state. The binding studies by researchers verified that, in addition to ion–dipole interactions, **DCVJ** forms a binding relationship with DNA through intercalation. This intercalation mechanism induces restriction in its excited-state twisting process, resulting in a substantial enhancement of its emission yield. Molecular docking studies further supported the intercalation mode of binding, revealing strong π–π stacking interactions and hydrogen bonding between **DCVJ** and guanine bases in DNA as key contributors to the intercalation process. Despite its relatively weak binding, the ultrafast molecular rotors were demonstrated as potential fluorescence sensors for DNA.

In 2023 Mondal and his co-workers presented the development and synthesis of three cationic julolidine–azolium conjugates (**OX-JLD (O)**, **BTZ-JLD (S)**, and **SEZ-JLD (Se)**) that act as fluorescent probes when interacting with RNA.[29] These conjugates exhibit high quantum yields and brightness, making them ideal for intracellular RNA imaging. Herein the authors discussed the design of three cationic julolidine–azolium conjugates that function as fluorescent probes for visualizing RNA in live cells. These probes exhibit a high level of brightness and quantum yields when they interact with RNA. The main focus of the study was to establish the potential use of these probes for intracellular RNA imaging. Among the probes, **BTZ-JLD** and **SEZ-JLD** show particularly promising photophysical properties and optical responses towards RNA. **BTZ-JLD** emits light at a longer wavelength in the red region of the electromagnetic spectrum when it interacts with RNA. These photophysical properties make **BTZ-JLD** a suitable candidate for fluorescence imaging of intracellular RNA in live cells.

A list of julolidine-based FMRs used for the detection of proteins and nucleic acids is provided in Fig. 5.

2.2 Nanoparticle and metal ion detection

Jha and his co-workers made the probe **PYJO4** which is equipped with several key features, including a unique pyrano[3,2-*c*]julolidin-2-one fluorophore based on TICT, selective ratiometric detection, and the ability to quantify and image intracellular Hg^{2+} in live cells with high sensitivity in the nano-molar range.[30] Upon binding of Hg^{2+} ions to the probe, a conformational change occurs, transitioning from a twisted state to a planar state. This change leads to a

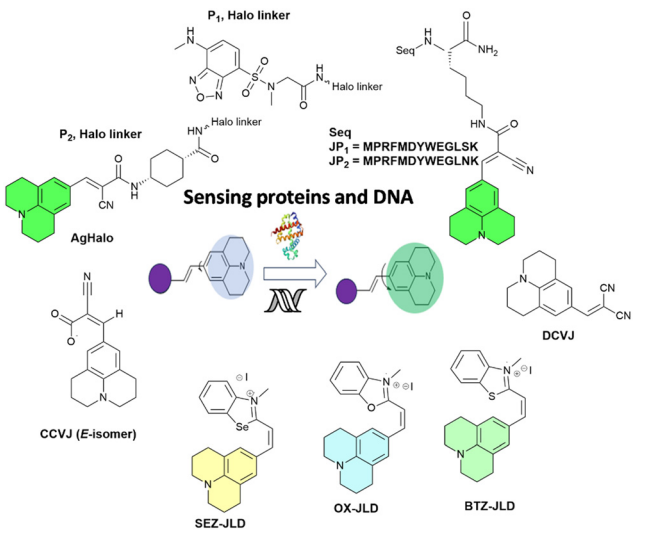

Fig. 5 Schematic representation and structures of the probes for sensing proteins and DNA.

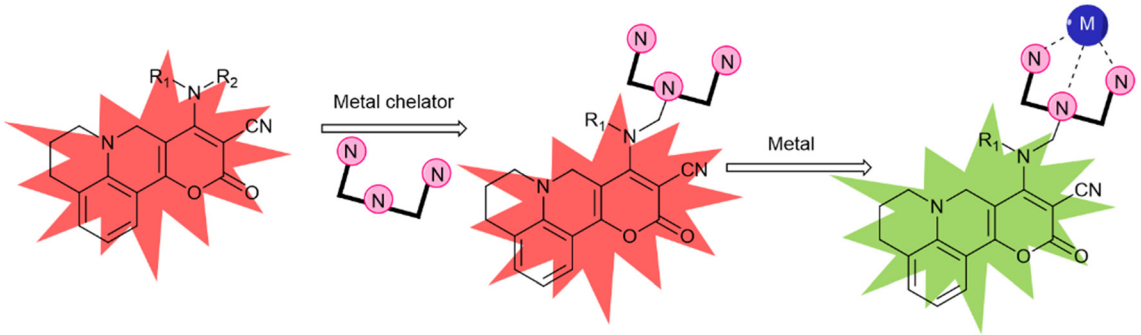

Fig. 6 A new strategy for developing a TICT based FMR for ratiometric sensing of metal ions. R_1 and R_2 are alkyl/functionalizable alkyl groups.

decrease in the intensity of the red emission band and an increase in the intensity of the green emission band (Fig. 6).

The conformational change induced by the binding of Hg^{2+} ions results in a significant alteration in the emission intensities. This enables the detection of Hg^{2+} ions even at low concentrations. To investigate the absorption and emission characteristics of compounds **PYJO1–PYJO4**, experiments were conducted in methanol/HEPES buffer (7 : 3) at pH 7.2. Among these compounds, **PYJO1** with a methylsulfanyl substitution displayed two absorption bands with peaks at 340 nm and 540 nm (Fig. 7a). However, it did not exhibit any fluorescence in the visible region. Fluorophores **PYJO2–PYJO4** display two absorption bands centered at 330 nm and 460–470 nm, corresponding to π–π* and n–π* transitions, respectively. The fluorescence spectra of **PYJO2–PYJO4** exhibit two emission bands centered at 481–530 nm (in the green region) and 645–680 nm (in the red region) (Fig. 7b). It is important to note that **PYJO4** demonstrates distinct dual emission characteristics, with a strong intensity band in the NIR region, which can be attributed to the effective TICT state.

The ratiometric response of fluorescence intensities (I_{530}/I_{665}) is enhanced from 0.7 to 4.2, resulting in a final enhancement factor of up to 6-fold. The detection limit is approximately 5.7×10^{-9} M (1.14 ppb). **PYJO4**-coated test strips offer a potential solution for detecting mercury ions in contaminated water. These strips provide a simple, rapid, and portable method for identifying the presence of toxic mercury ions. When exposed to mercury ions, the test strips undergo a noticeable fluorescence change from red to green, enabling easy visual detection. The sensitivity of the test strips has been demonstrated up to a level of 200 ppb. The successful application of **PYJO4** in detecting and imaging intracellular Hg^{2+} in live MCF-7 breast cancer cells has been demonstrated.

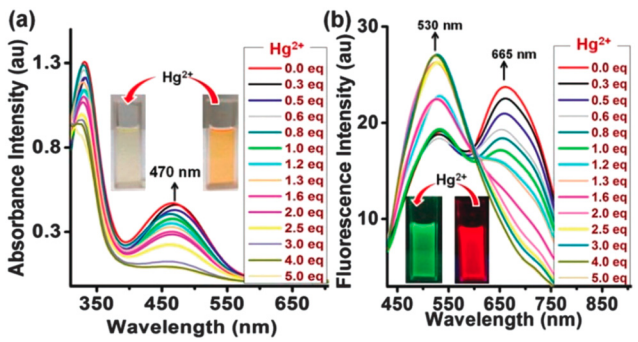

Fig. 7 (a) Absorption spectra in the visible light and (b) ratiometric fluorescence spectra with increasing concentration of the metal. Insets show color change upon addition of Hg^{2+} ions under daylight (for Fig. a) and under UV light (for Fig. b). Reprinted with permission from ref. 30. Copyright 2016. Royal Society of Chemistry.

A fluorescent molecular rotor is utilized in a method to detect and measure polystyrene nanoparticles.[31] The probe's fluorescence quantum yield is altered when polystyrene nanoparticles are present. In 2021 Moraz and his co-workers were able to successfully detect and measure polystyrene nanoparticles in water, and they also determined the range for detection and quantification for specific nanoparticle sizes.[31] This method is significant because it allows for the assessment of the presence and concentration of polystyrene nanoparticles in biological samples and environmental water. These nanoparticles are a major threat to aquatic and terrestrial environments due to their potential to harm wildlife and ecosystems. The study also investigated the influence of temperature and viscosity on the detection and quantification of polystyrene nanoparticles (Fig. 8). The results showed that temperature did not significantly affect the detection and quantification of polystyrene nanoparticles, while viscosity did not affect the fluorescence of **DCVJ** in the presence of polystyrene nanoparticles. The hydrophobic interaction between **DCVJ** and the polystyrene nanoparticles was found to be the main factor influencing the detection and quantification of polystyrene nanoparticles.

A new analytical method for detecting and quantifying PSNs using an FMR has been developed. The method uses a three-unit molecular system, **DCVJ**, a commercially available FMR, to determine the concentration of nanosized plastic beads. The underlying phenomenon is a hydrophobic interaction between the probe and the analyte, rather than the viscosity resulting from the presence of the nanomaterial. The most suitable method is the appearance and increase in a second band at 620 nm due to hydrophobic interactions possibly associated with the excimeric feature within the beads. The surface area and particle size also play a role in

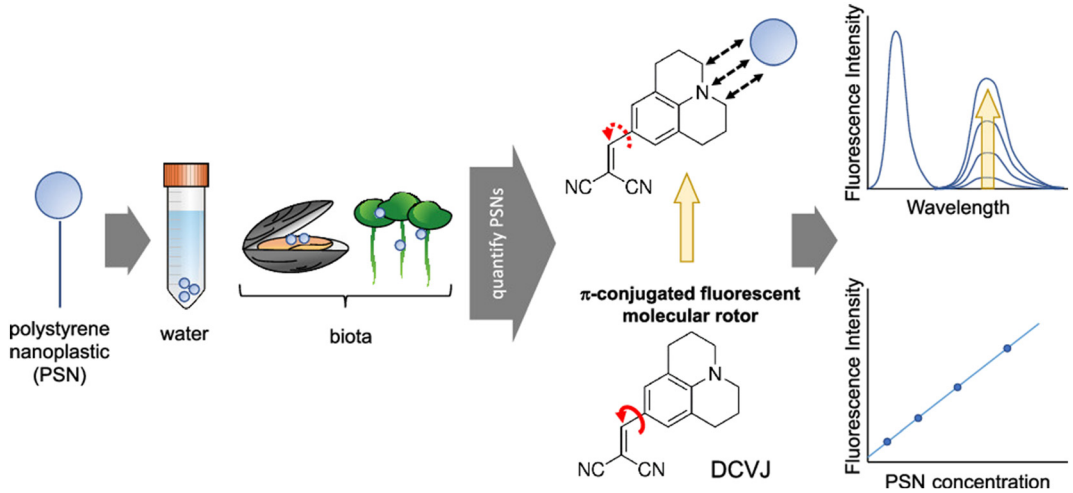

Fig. 8 Detection of polystyrene nanoplastic (PSNs) using a **DCVJ**-based FMR. Reprinted with permission from ref. 31. Copyright 2021. American Chemical Society.

the fluorescence. The method is label-free and easy to implement, but further investigation is needed to reach standardization for routine analysis. This work presents the feasibility of quantifying PSNs using **DCVJ** fluorescence and opens new perspectives in this field.

2.3 Self-assembly and aggregation-induced emission

In 2018 Guazzelli and his co-workers synthesized a fluorescent molecular rotor monomer utilized as a fluorescent label to investigate the self-assembly behavior in a water solution with varying temperatures.[32] However, while studies on fluorescence emission have been conducted for ionic amphiphilic random copolymers containing covalently linked fluorophores, there is limited knowledge regarding the physical dispersion of fluorophores in non-ionic random copolymers (Fig. 9a). In dilute solutions, FMRs can assume a non-emissive TICT state, but in aggregates, the TICT state is suppressed in favor of the radiative emitting locally excited (LE) state.

The terpolymer was designed to have a PEGMA : FA co-unit content of 75 : 25 mol% : mol%, ensuring solubility in water and organic solvents, while the **JCBF** co-unit content of approximately 1 mol% ensured UV light absorption–emission from isolated FMR labels.

The fluorescent probe **JCBF** was covalently anchored due to its poor solubility in water. The **JCBF** content was determined by UV absorption measurements of terpolymer solutions in chloroform. The **JCBF** chromophore exhibited no significant variation in its spectroscopic properties when incorporated in the amphiphilic polymer. The terpolymer consisted of 74, 25, and 1 mol% of PEGMA, FA, and **JCBF**, respectively, and was named PEGMA74-*co*-FA25-*co*-JCBF1.

The fluorescence emission intensity of the terpolymer is higher in water compared to organic solvents because of the preferential encapsulation of the hydrophobic **JCBF** co-units within the hydrophobic compartments of the terpolymer (Fig. 9a). This leads to a reduction in their degree of mobility, resulting in an increased intensity of fluorescence emission. Additionally, the hydrophilic PEGMA chains of the terpolymer maximize contact with water, further enhancing the fluorescence emission intensity (Fig. 9b). Its thermo-responsive behavior in water is demonstrated through DLS,

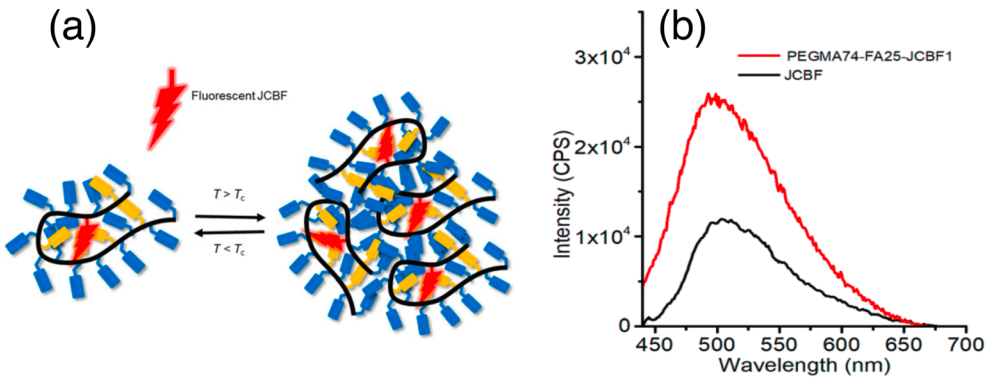

Fig. 9 (a) Schematic representation of monitoring the phase transition of a unimer micelle to multichain aggregates using **JCBF** as a molecular rotor, and (b) emission spectra of **JCBF** and PEGMA74-FA25-JCBF1 in $CHCl_3$. Reprinted with permission from ref. 32. Copyright 2018. Wiley VCH.

UV-vis, and fluorescence spectroscopy measurements. This design and synthesis could be useful for advanced applications, such as controlled drug delivery systems.

In 2018 Mori and his co-workers used 9-(dicyanovinyl) julolidine (**DCVJ**) and its derivatized form, 9-(2-carboxy-2-cyanovinyl)julolidine (**CCVJ**), belonging to a group of TICT-type fluorophores that serve as representative examples.[33] The authors here focused on the rotation of molecules in either a two-dimensional monolayer or a three-dimensional collapsed film at an air–water interface. By employing fluorescence spectroscopy, the researchers investigated the rotational behavior of specific molecules. They discovered that as viscosity increased, the fluorescence intensity also increased, indicating a hindrance in internal molecular rotations. Furthermore, the emissions from the monolayers remained suppressed until the monolayers collapsed. To measure the rotation of molecules in the monolayer or collapsed film, *in situ* fluorescence spectroscopy was employed. The researchers observed no excimeric emission even after monolayer compression indicating free intramolecular rotation.

When the molecules are placed in a less viscous solvent, they have the ability to rotate within themselves, resulting in a decrease in the intensity of fluorescence. On the other hand, when the molecules are in a more viscous solvent, their rotation is hindered, leading to an increase in fluorescence intensity (Fig. 10). This interesting phenomenon can be utilized to monitor the internal motion of the molecules. In a study focused on the rotation of molecules at the air–water interface, it was discovered that the collapse of the monolayers resulted in the suppression of emissions. Before the collapse of the monolayers, no fluorescence was observed for **CCVJ-C12** or **CCVJ-Chol**. However, after the collapse of the monolayers, clear emission from the monomers was observed when **CCVJ-C12** was dispersed in glycerol. This confirmed that the observation of monomer fluorescence was possible with the specific quantity of molecules used, as long as intramolecular rotation was inhibited. The transferred film was analyzed for its morphological and fluorescence properties. From the AFM images, no significant changes in morphology were observed before and after the collapse of the monolayers. The fluorescence properties of the LB films were also analyzed. Prior to the collapse, the LB film of the monolayer did not exhibit monomer fluorescence, indicating that the intramolecular rotation of molecules was not inhibited in the LB film. However, the collapsed film showed excimer emission at 600 nm, similar to the collapsed monolayer at the air–water interface.

This study demonstrates that TICT-type lipophilized fluorescent rotors in monolayers at the air–water interface are capable of free intramolecular rotation, as evidenced by the absence of fluorescence emission indicative of rotation inhibition. However, when subjected to in-plane compression resulting in monolayer collapse, rotation was inhibited and excimer emission was observed. The proposed mechanism for monolayer collapse involves protrusion of the monolayer to the air side, where hydrophilic chromophores interact and inhibit internal molecular rotation. A list of julolidine-based FMRs used for understanding self-assembly and aggregation-induced emission properties is provided in Fig. 11.

2.4 Viscosity sensing of the microenvironment

In 2015, Zhang and co-workers modified the classical molecular rotor **DCVJ** by substituting the acceptor's two

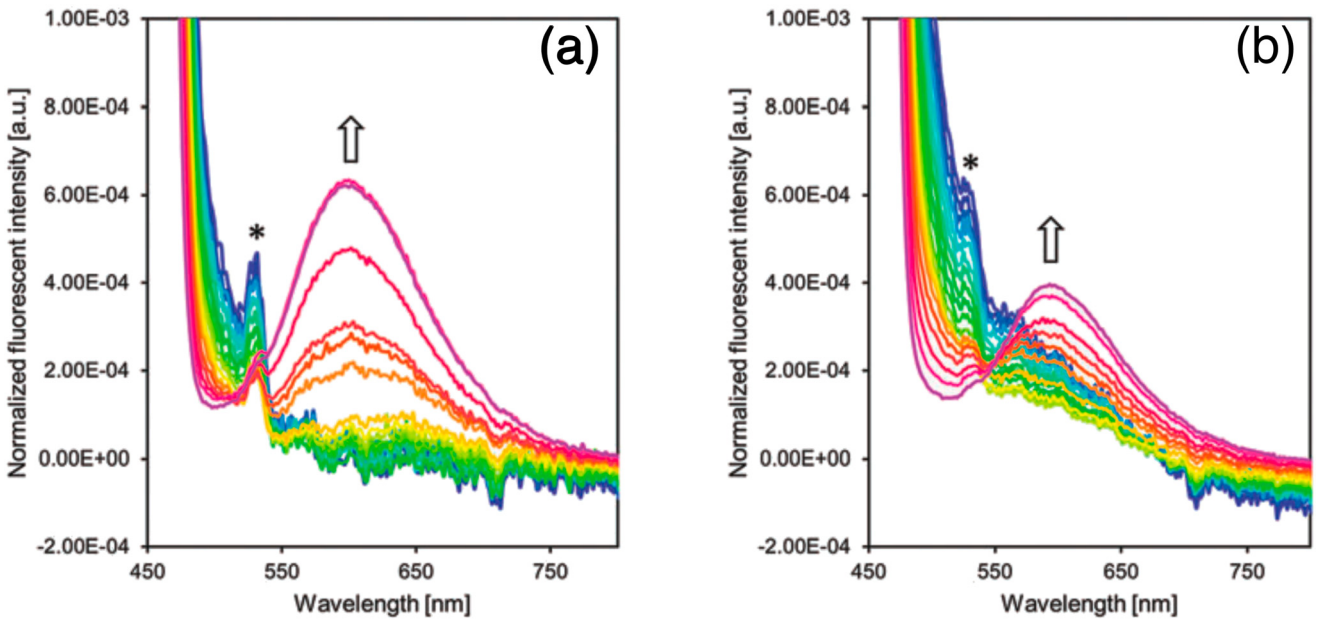

Fig. 10 (a) Fluorescence emission spectra of **CCVJ-C12** (left) and (b) **CCVJ-Chol** (right) at surface pressure from 0 to over 50 mN m^{-1}. Reprinted with permission from ref. 33. Copyright 2018. Royal Society of Chemistry.

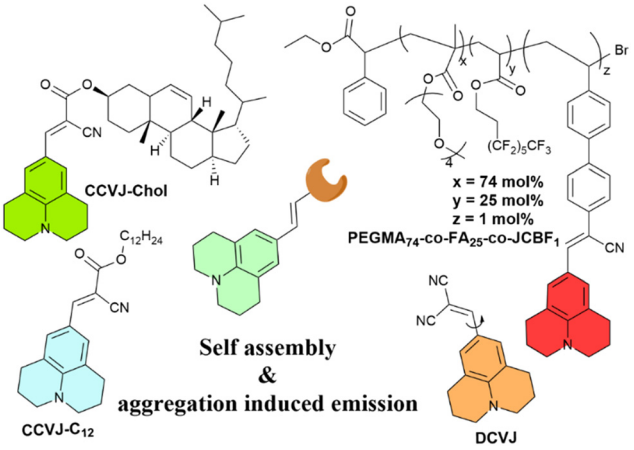

Fig. 11 Schematic representation and structures of the probes for self-assembly and aggregation induced emission.

nitrile groups with a pyridinium cationic group.[34] This substitution caused a shift in the emission maxima of the probe to 620 nm and is also suitable for application in two-photon microscopy using a 10 mW beam at 900 nm. The introduction of the cationic group endowed the probe with mitochondria-targeting capabilities due to the negative membrane potential of mitochondria. The synthesized probe, leveraging its molecular rotor properties, exhibited sensitivity to viscosity and offered an improved signal-to-noise ratio. The authors investigated the probe's utility in imaging mitochondria in cancerous, as well as various normal cell lines, and its potential for application in two-photon microscopy. The localization of the probe was dependent on the negative potential of the mitochondria, as evidenced by experiments using mitochondria uncoupler CCCP.

Chwastek and his co-workers in 2020 proposed a method using fluorescence correlation spectroscopy (FCS) to estimate the diffusivity of a molecular probe.[35] FCS can provide a quantitative measure of probe diffusivity, which can be related to the viscosity of the medium. The dye **DCVJ** is located in the vicinity of the glycerol backbone of phospholipids rather than around the terminal methyl moiety of acyl chains. Its high sensitivity to the cholesterol content of the lipid membrane indicates its preferential localization in the proximity of membrane cholesterol. The stable localization of the dye close to the cholesterol pocket of the lipid membrane is supported by the lack of noticeable changes in the emission spectra of **DCVJ** for different membrane compositions and temperatures. Finally, the comparison between *Mycoplasma mycoides* membranes and artificial lipid mixtures showed that at temperatures equal to or above the growth conditions, the bacterial membranes have a very similar viscosity and temperature dependence to that of the liquid-disordered (L_d) state artificial lipid mixture. However, at temperatures below the growth conditions, the viscosity of the bacterial membranes approaches the values of the liquid-ordered (L_o) phase of the artificial lipid mixture, indicating a more viscous state. This suggests that the lipid membrane of *Mycoplasma mycoides* exists in the fluid (L_d) state at and above the growth temperature, and transforms into a more viscous (L_o) phase at temperatures about 10 degrees below the growth temperature.

PDT has emerged as a promising theranostic approach with notable advantages such as spatial–temporal controllability, non-invasiveness, and minimal drug resistance.[36] The development of new photosensitizers (PSs) with unique properties has garnered significant attention. Extensive efforts have been dedicated to creating PSs with high efficiency in producing singlet oxygen ($^1O_2$), the ability to target specific organelles, and absorption in the red to near-infrared (NIR) range. Among the organelle-targeting PSs, those that target mitochondria can greatly enhance the photodynamic effect due to the pivotal role of mitochondria in cellular function and their association with cell apoptosis. Monitoring the dynamics of mitochondrial viscosity is crucial as it is closely linked to respiratory state and mitochondrial metabolism. Numerous methods have been established for this purpose.

Recently, two dual functional PSs were reported, capable of targeting mitochondria and exhibiting a 'turn-on' fluorescence response to changes in viscosity.[36] It is noteworthy that CCVJ-Mito-2, one of the PSs, has absorption in the NIR region, making it more suitable for *in vivo* PDT applications (Fig. 12). These two PSs were successfully employed to detect viscosity changes in mitochondria and demonstrated phototoxicity to cancer cells even at extremely low concentrations. CCVJ-Mito-1 and CCVJ-Mito-2 were synthesized through a Knoevenagel condensation reaction. CCVJ-Mito-1 exhibited maximum absorption around 600 nm, while CCVJ-Mito-2 showed a longer absorption wavelength at approximately 680 nm in water due to an extended conjugation system. In glycerol, both PSs exhibited a bathochromic shift in absorption compared to water, which could be attributed to suppressed intramolecular rotation (Fig. 13a and b). Importantly, the fluorescence signal of CCVJ-Mito-1 and CCVJ-Mito-2 did not significantly enhance in the presence of other common biomolecules, indicating their good selectivity towards viscosity.

The fluorescence of CCVJ-Mito-1 and CCVJ-Mito-2 remains largely unaffected by changes in pH, making them suitable for use in complex biological environments. This

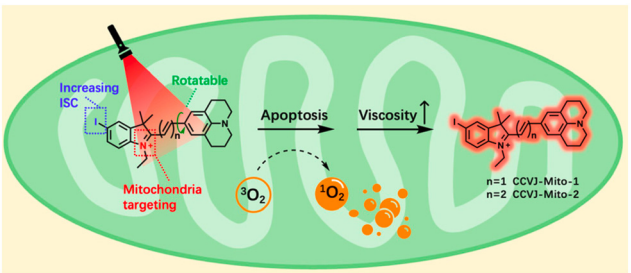

Fig. 12 Structure design of dual functional PSs and synchronous mitochondrial viscosity dynamic imaging. Reprinted with permission from ref. 36. Copyright 2022. Royal Society of Chemistry.

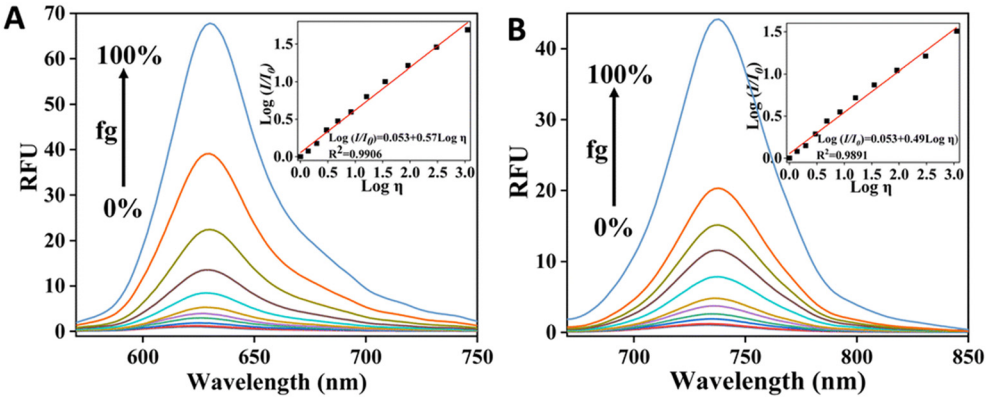

Fig. 13 Fluorescence response of CCVJ-Mito-1 (A) & CCVJ-Mito-2 (B) towards viscosity variation by changing glycerol fraction (f_g). Inset show the validation of Förster–Hoffmann equation. Reprinted with permission from ref. 36. Copyright 2022. Royal Society of Chemistry.

characteristic, combined with the fact that the fluorescence of these PSs overlaps with that of MitoTracker Green-FM in HeLa cells and other types of cancer cells, suggests that both CCVJ-Mito-1 and CCVJ-Mito-2 have the potential to target mitochondria. Additionally, these two dual functional PSs have been successfully developed to not only efficiently perform photodynamic therapy on cancer cells but also monitor changes in mitochondrial viscosity in real-time.

The authors have successfully created two PSs, CCVJ-Mito-1 and CCVJ-Mito-2, that have dual functionality. These PSs are capable of effectively carrying out PDT on cancer cells while simultaneously monitoring the viscosity dynamics of mitochondria. Our team is confident that these PSs will aid in our understanding of the changes that occur in the intracellular microenvironment during PDT and will guide future PDT processes. Of particular interest is PS CCVJ-Mito-2, which has NIR absorption and holds great potential for *in vivo* biological applications. We are currently conducting relevant studies on this PS.

Our research group has designed molecular rotors based on julolidine to investigate the viscosity of subcellular compartments. To achieve a far-red emission, we extended the conjugation between the julolidine donor and dinitrile acceptor groups. The acceptor group was attached with a tolyl group or indoline group, as introduction of a bulkier indoline group enhances the viscosity sensitivity of the rotor. Further, organelle targeting moieties are attached to specifically localize the rotor to the particular target in the cells. **Jind-mor** has been conjugated with a morpholine group to guide the molecule to the lysosomal compartment of the cells.[37] It was utilized to monitor the lysosomal stress in live cells and osmotic stress in *C. elegans*. In another variation, we modified the rotor by introducing a trimethyl ammonium cationic group, guiding the resulting **JMT** rotor to the mitochondria of cells.[38] **JMT** was then utilized to assess mitochondrial stress, leveraging the fact that under stress conditions, the viscosity of mitochondria tends to increase. Researchers have documented a distinct form of cell death called ferroptosis, which is dependent on iron and differs in appearance and biochemical characteristics from apoptosis, necrosis, and autophagy. This unique process plays a crucial role in the development of various diseases and has emerged as a significant area of research for improving the treatment and prognosis of related conditions. During ferroptosis, the depletion of intracellular glutathione (GSH) leads to a decrease in the activity of glutathione peroxidase (GPX4). As a result, lipid peroxides cannot be metabolized through the GPX4-catalyzed reduction reaction, while Fe^{2+} continuously oxidizes lipids in a manner similar to the Fenton reaction, leading to the generation of a substantial amount of reactive oxygen species (ROS) that promote ferroptosis. In order to regulate ER homeostasis, ER stress triggers ER-associated degradation. ER-phagy, a newly identified type of autophagy, eliminates damaged ER caused by excessive ER stress and safeguards cells from additional harm. When ER stress occurs, misfolded and unfolded proteins accumulate in the ER, leading to an elevation in ER viscosity.[39] A list of julolidine-based far-red emissive FMRs used for

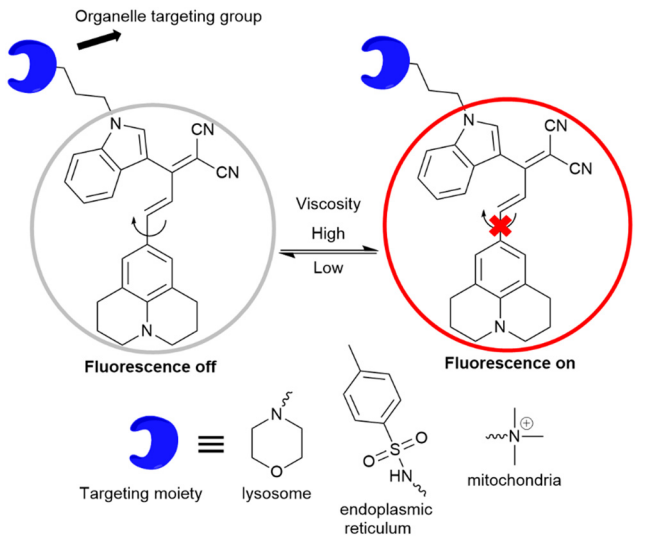

Fig. 14 Schematic view of viscosity response to an organelle targeting molecular rotor.

understanding sub-cellular organelle viscosity under stress conditions is provided in Fig. 14.

Fluorescence bioimaging is an effective technique for tracking subcellular viscosity, offering numerous benefits including noninvasiveness, speed, real-time monitoring, and spatiotemporal imaging. In this study, the researchers have successfully designed and synthesized a molecular rotor that is sensitive to viscosity, enabling the monitoring of endoplasmic reticulum (ER) changes during various modes of biological cell death. To specifically target the ER, derivatives of sulphonylurea were employed, as the ER lumen contains sulphonamide receptors. The synthesized probe, named **JER**, was modified with *p*-toluene sulphonamide to serve as the recognition component for the ER.[39]

The absorption peak was observed at a wavelength of 540 nm, while the emission peak occurred at 644 nm. Additionally, the excitation peak was also observed at 540 nm when using DMSO as the solvent. The absorption and excitation spectra showed a good overlap, indicating the presence of a single emitting chromophore with high optical purity.

The emission behavior of **JER** in different solvents revealed that it exhibited significant fluorescence intensity in highly viscous solvents, while a weak fluorescence was observed in low viscosity solvents. This can be attributed to the presence of a conjugated double bond between the donor and acceptor, which regulates the emission properties of the probe in solutions with varying viscosity. Furthermore, a remarkable 400-fold increase in fluorescence intensity was observed with increasing glycerol percentage in water. The fluorescence intensity at 645 nm was well-fitted by the Förster–Hoffmann equation, $\log I = x \log Z + \log C$. A strong linear relationship (R^2 = 0.98) was found within the viscosity range of 2 to 905 cP. Importantly, this linear relationship over a wide viscosity range suggests that **JER** has the potential to be used as a fluorophore for measuring cellular microviscosity. Additionally, fluorescence measurements were also conducted using varying percentages of methanol in glycerol with similar polarity. A list of julolidine-based FMRs used for understanding sub-cellular viscosity is provided in Fig. 15.

The emission properties of **JER** were also analyzed by the author in relation to pH for potential use in a biological setting. By examining the fluorescence properties of **JER** in various pH solutions with an intracellular viscosity of approximately 156 cP, we were able to determine its pH tolerance. The probe also demonstrated remarkable photostability when exposed to continuous irradiation (90 lx) from a 450 W xenon lamp for up to 60 minutes. These findings establish **JER** as a suitable tool for investigating viscosity in a biological environment.

2.5 Julolidine-based FMRs for understanding polymer properties

Local microenvironmental properties associated with the polymerization process are not accessible from macroscopic measurements. However, julolidine-based fluorescent

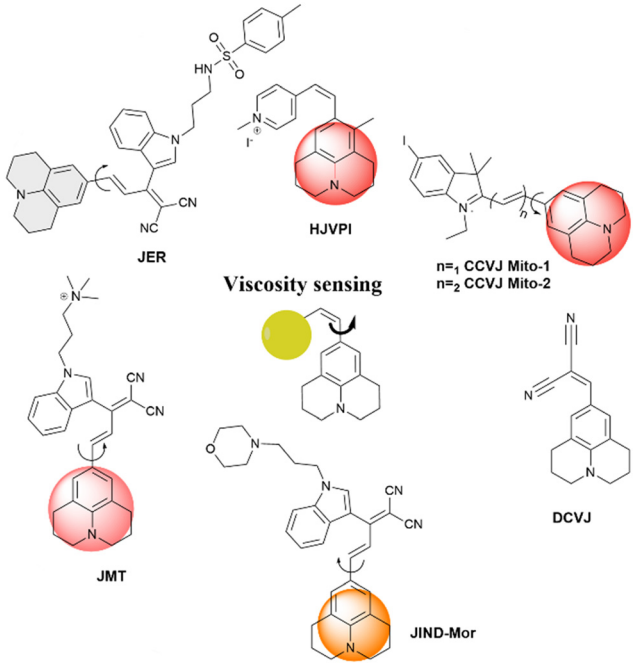

Fig. 15 Schematic representation and structures of the probes for viscosity sensing.

molecular rotors incorporated in polymer matrices can be utilized to probe the local dynamical changes of the polymer matrix. The viscosity-induced change in the emission property of the molecular rotor can be utilized to understand the free-volume related properties of the polymer such as phase transition, fluidity, glass transition temperature, and physical aging. The emission change of molecular rotors has a quantitative relationship with the local fluidity of the polymer matrix and this is generally applicable to a wide range of polymer types.

In 2016, Joly and co-workers investigated the solid-state polymerization (SSP) process of poly(butylene succinate) (PBS) by utilizing the emission properties of a 9-(2-carboxy-2-cyanovinyl)julolidine (**CCVJ**) molecular rotor.[40] The emission of **CCVJ** was dependent on both the molecular weight of the

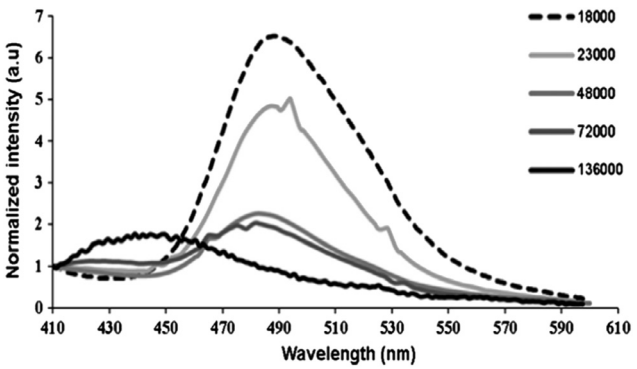

Fig. 16 Emission spectra of CCVJ embedded in PBS of different molecular weights (M_w). Reprinted with permission from ref. 40. Copyright 2016. Elsevier.

polymer and the local polarity of the polymer. The emission maximum of **CCVJ** shows a strong blue shift with a decrease when the M_w increased. The observation was attributed to the local polarity change of the PBS medium around the **CCVJ** probe. The shorter polymeric chains exhibited a higher acidic index (AI) value and consequently a higher medium polarity. As demonstrated in Fig. 16, the decline in the fluorescent intensity and associated blue shift are because of the increase in PBS molecular weight. According to these results, CCVJ can be employed to monitor the SSP process kinetics.

Andrea Pucci and his colleagues have used AIEgens as fluorescent probes for monitoring the polymerization of 4,4′-methylenediphenyl diisocyanate (MDI) and polyethylene glycol to form polyurethane in a dimethylacetamide solution.[41] The polymerization kinetics was effectively monitored from the viscosity variation associated with the degree of polymerization. The variation of viscosity due to the polymerization process was monitored using the relative fluorescence variation of the **DCVJ**-based fluorescent molecular rotor using an optical fiber based excitation connected to a spectrofluorometer. The fluorescence change in the **DCVJ** rotor probe matches well with the viscosity variation due to the polymerization process as shown in Fig. 17.

In 2020, Yao *et al.* investigated the fluorescence emission of a CCVJ-based molecular rotor to differentiate glucan polymers with different branch structures. The authors have prepared amylopectin, phytoglycogen, and their β-limit dextrins as glucan models, and incorporated **CCVJ** as a hydrophilic molecular rotor.[42] The viscosities of dilute glucan dispersions were determined and the fluorescence response of **CCVJ** in these dispersions was measured (Fig. 18). The emission **CCVJ** showed a linear correlation with glucan content. The plot of fluorescence emission response of **CCVJ** against branch concentration (C_b) shows linear dependence for diluted glucan dispersions. Hence, the FMR can be used as an analytical tool for differentiating different branch structures of biopolymers.

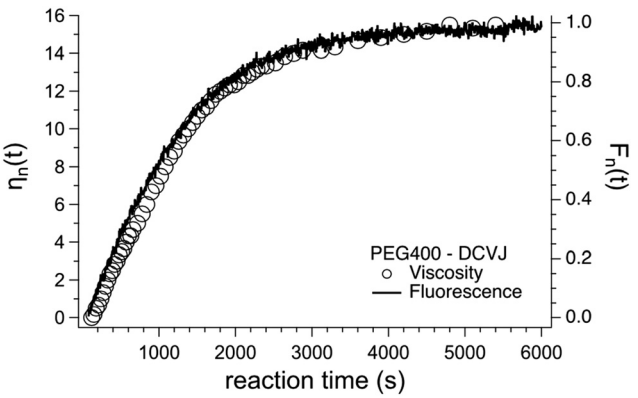

Fig. 17 Monitoring the synthesis of polyurethane (PU) in the presence of 9-(2,2-dicyanovinyl)julolidine (**DCVJ**). Relative viscosity variations ($\eta_n(t)$) and relative fluorescence variations ($F_n(t)$) are shown in open circles and a solid line, respectively.

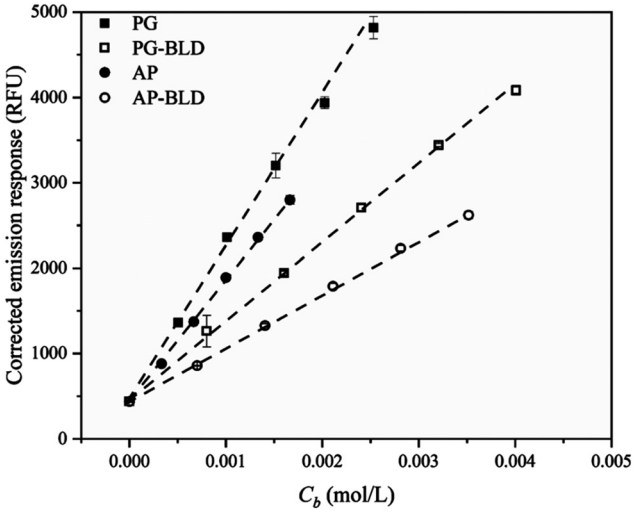

Fig. 18 Corrected fluorescence emission response of **CCVJ** in diluted glucan dispersions as a function of branch concentration (C_b). Reprinted with permission from ref. 42. Copyright 2020. Elsevier.

Andrea Pucci and co-workers have reported polystyrene copolymers containing julolidine fluorescent molecular rotors (**JCAEM**) to develop vapochromic films for detecting volatile organic compounds (VOCs).[43] Poly(styrene-*co*-hydroxyethylmethacrylate) copolymers functionalized with **JCAEM** (P(STY-*co*-JCAEM)), exhibited viscosity-dependent emission properties when exposed to saturated atmospheres of VOCs which interacted well with the emission reporter. The authors observed a pronounced decrease in the emission intensity (Fig. 19) due to the solvent-induced changes in the local viscosity of the medium. As expected, the response appeared faster and more pronounced (Fig. 19) for copolymers with the lowest **JCAEM** content. A significant vapochromism was observed when exposed to Et_2O and CH_2Cl_2 vapours due to strong deactivation pathways of the **JCAEM** units in the presence of VOCs. This phenomenon was attributed to the role of the covalent approach for **JCAEM** moiety distribution in the polymer matrix.

3. Conclusion and future outlook

The photo-isomerization process of **CCVJ** is limited in biomimetic and biological nano-cavities, affecting protein misfolding and aggregation. A new probe for long-term RNA trafficking, **SEZ-JLD**, has been developed, revealing new possibilities for understanding metal ion biotoxicity mechanisms. A new analytical method for detecting and quantifying polystyrene nanoplastic has been developed. A fluorescently-labeled amphiphilic terpolymer was created using ATRP, incorporating a julolidine-based FMR monomer for fluorescence response. Another study demonstrated that TICT-type lipophilized fluorescent rotors can perform free intramolecular rotation, and measurements can identify liquid–liquid phase transitions in *M. mycoides*. Two photosensitizers, CCVJ-Mito-1 and CCVJ-Mito-2, have

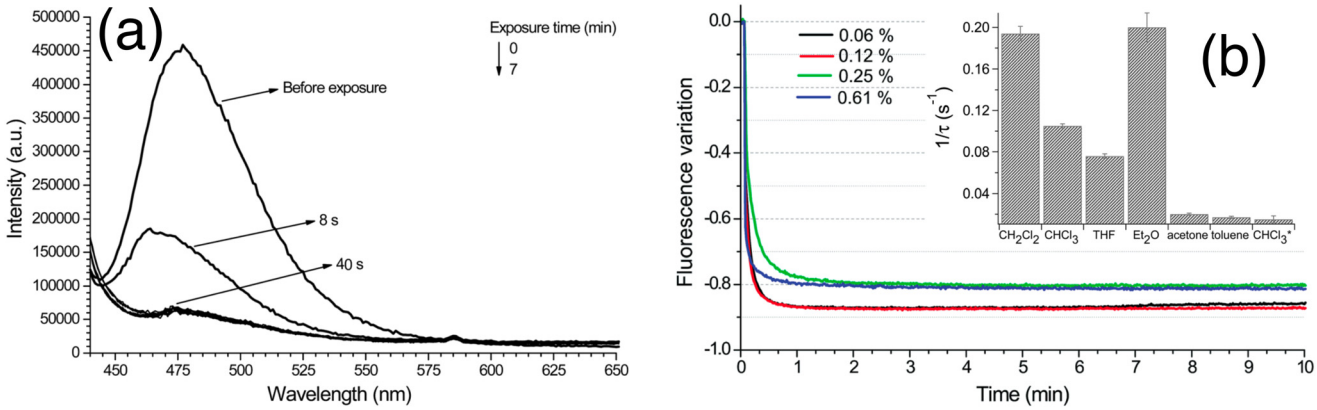

Fig. 19 (a) Quenching of fluorescence emission of the P(STY-*co*-JCAEM) film (0.06 mol% **JCAEM**) as a function of exposure to chloroform vapors; (b) variation in the fluorescence maximum intensity with exposure time to chloroform vapors for all P(STY-*co*-JCAEM) (mol% of **JCAEM**) films; the inset shows the rate constant of the attenuation of emission intensity. Reprinted with permission from ref. 43. Copyright 2017. Royal Society of Chemistry.

displayed potential for photodynamic therapy on cancer cells and were also utilized for real-time monitoring of mitochondrial viscosity. Researchers have successfully modified the traditional **DCVJ** molecular rotor to enhance its photophysical properties, focusing primarily on alterations in the acceptor part. These modifications aim to induce a red shift in emission or target specific locations based on the intended application. The evolution of diverse julolidine-based molecular rotor designs holds significant promise for advancing possibilities in various fields such as biological research, membrane sensing, metal ion detection, unlabeled nanoparticle detection and quantification, human microglobulin oligomerization at low pH, two-photon microscopy, and viscosity measurement.

This review provides a comprehensive overview of current research in this field and discusses the potential for future advancements. Notably, the exploration of viscosity changes throughout different phases of the cell cycle and their implications in developmental biology remains an unexplored avenue using julolidine-based molecular rotors. Additionally, these rotors can be employed to investigate remote and inaccessible local environmental parameters, including viscosity and pressure. Further advancements in modifying julolidine-based molecular rotors to emit in the far-red or near-infrared spectrum, coupled with good solubility, could unlock numerous possibilities for practical applications in real-world scenarios.

Conflicts of interest

There are no conflicts to declare.

Acknowledgements

We wish to acknowledge the contribution of all researchers working on julolidine for their passion and hard work for the development of beautiful julolidine chemistry. NC would like to thank IISERB Bhopal for her doctoral fellowship. We acknowledge the financial support from IISER Bhopal.

References

1 L. L. Wu, J. H. Liu, P. Li, B. Tang and T. D. James, *Chem. Soc. Rev.*, 2021, **50**, 702–734.
2 J. L. Yin, L. Huang, L. L. Wu, J. F. Li, T. D. James and W. Y. Lin, *Chem. Soc. Rev.*, 2021, **50**, 12098–12150.
3 J. Eckmann, S. H. Eckert, K. Leuner, W. E. Muller and G. P. Eckert, *Int. J. Biochem. Cell Biol.*, 2013, **45**, 76–80.
4 H. Singh, K. Tiwari, R. Tiwari, S. K. Pramanik and A. Das, *Chem. Rev.*, 2019, **119**, 11718–11760.
5 K. Pal, I. Samanta, R. K. Gupta, D. Goswami and A. L. Koner, *Chem. Commun.*, 2018, **54**, 10590–10593.
6 In *Principles of Fluorescence Spectroscopy*, ed. J. R. Lakowicz, Springer US, Boston, MA, 2006, pp. 331–351.
7 L. L. Wu, C. S. Huang, B. Emery, A. C. Sedgwick, S. D. Bull, X. P. He, H. Tian, J. Yoon, J. L. Sessler and T. D. James, *Chem. Soc. Rev.*, 2020, **49**, 5110–5139.
8 C. Wang, W. J. Chi, Q. L. Qiao, D. V. Tan, Z. C. Xu and X. G. Liu, *Chem. Soc. Rev.*, 2021, **50**, 12656–12678.
9 A. C. Sedgwick, L. L. Wu, H. H. Han, S. D. Bull, X. P. He, T. D. James, J. L. Sessler, B. Z. Tang, H. Tian and J. Yoon, *Chem. Soc. Rev.*, 2018, **47**, 8842–8880.
10 T. Dutta, K. Pal and A. L. Koner, *Chem. Rec.*, 2022, **22**, e202200035.
11 D. Su, C. L. Teoh, L. Wang, X. Liu and Y.-T. Chang, *Chem. Soc. Rev.*, 2017, **46**, 4833–4844.
12 S. C. Lee, J. Heo, H. C. Woo, J. A. Lee, Y. H. Seo, C. L. Lee, S. Kim and O. P. Kwon, *Chem. – Eur. J.*, 2018, **24**, 13706–13718.
13 T. Dutta, S. Das, I. Gupta and A. L. Koner, *Chem. Sci.*, 2022, **13**, 12987–12995.
14 M. A. Haidekker, T. Ling, M. Anglo, H. Y. Stevens, J. A. Frangos and E. A. Theodorakis, *Chem. Biol.*, 2001, **8**, 123–131.
15 M. A. Haidekker, T. P. Brady, D. Lichlyter and E. A. Theodorakis, *J. Am. Chem. Soc.*, 2006, **128**, 398–399.

16 M. A. Haidekker and E. A. Theodorakis, *J. Mater. Chem. C*, 2016, **4**, 2707–2718.
17 M. A. Haidekker and E. A. Theodorakis, *Org. Biomol. Chem.*, 2007, **5**, 1669–1678.
18 L. S. Kocsis, K. M. Elbel, B. A. Hardigree, K. M. Brummond, M. A. Haidekker and E. A. Theodorakis, *Org. Biomol. Chem.*, 2015, **13**, 2965–2973.
19 W. L. Goh, M. Y. Lee, T. L. Joseph, S. T. Quah, C. J. Brown, C. Verma, S. Brenner, F. J. Ghadessy and Y. N. Teo, *J. Am. Chem. Soc.*, 2014, **136**, 6159–6162.
20 K. Gavvala, S. Satpathi and P. Hazra, *RSC Adv.*, 2015, **5**, 72793–72800.
21 D. Narang, A. Singh, H. M. Swasthi and S. Mukhopadhyay, *J. Phys. Chem. A*, 2016, **120**, 7815–7823.
22 S. Nagarajan and L. J. Lapidus, *ChemBioChem*, 2017, **18**, 2205–2211.
23 M. Fares, Y. H. Li, Y. Liu, K. Miao, Z. Gao, Y. F. Zhai and X. Zhang, *Bioconjugate Chem.*, 2018, **29**, 215–224.
24 Y. Bai, W. Wan, Y. Huang, W. Jin, H. Lyu, Q. Xia, X. Dong, Z. Gao and Y. Liu, *Chem. Sci.*, 2021, **12**, 8468–8476.
25 K. H. Jung, S. F. Kim, Y. Liu and X. Zhang, *ChemBioChem*, 2019, **20**, 1078–1087.
26 D. Zhang, Z. Chen, Z. Du, B. Bao, N. Su, X. Chen, Y. Ge, Q. Lin, L. Yang, Y. Hua, S. Wang, X. Hua, F. Zuo, N. Li, R. Liu, L. Jiang, C. Bao, Y. Zhao, J. Loscalzo, Y. Yang and L. Zhu, *Cell Discovery*, 2023, **9**, 56.
27 K. H. Jung, M. Fares, L. S. Grainger, C. H. Wolstenholme, A. Hou, Y. Liu and X. Zhang, *Org. Biomol. Chem.*, 2019, **17**, 1906–1915.
28 R. Kalel, A. K. Mora, R. Ghosh, D. D. Dhavale, D. K. Palit and S. Nath, *J. Phys. Chem. A*, 2016, **120**, 9843–9853.
29 I. C. Mondal, P. Rawat, M. Galkin, S. Deka, A. Karmakar, P. Mondal and S. Ghosh, *Org. Biomol. Chem.*, 2023, **21**, 7831–7840.
30 A. K. Jha, S. Umar, R. K. Arya, D. Datta and A. Goel, *J. Mater. Chem. B*, 2016, **4**, 4934–4940.
31 A. Moraz and F. Breider, *Anal. Chem.*, 2021, **93**, 14976–14984.
32 E. Guazzelli, E. Masotti, T. Biver, A. Pucci, E. Martinelli and G. Galli, *J. Polym. Sci., Part A: Polym. Chem.*, 2018, **56**, 797–804.
33 T. Mori, H. Komatsu, N. Sakamoto, K. Suzuki, J. P. Hill, M. Matsumoto, H. Sakai, K. Ariga and W. Nakanishi, *Phys. Chem. Chem. Phys.*, 2018, **20**, 3073–3078.
34 G. Zhang, Y. M. Sun, X. Q. He, W. J. Zhang, M. G. Tian, R. Q. Feng, R. Y. Zhang, X. C. Li, L. F. Guo, X. Q. Yu and S. L. Zhang, *Anal. Chem.*, 2015, **87**, 12088–12095.
35 G. Chwastek, E. P. Petrov and J. P. Sáenz, *ChemBioChem*, 2020, **21**, 836–844.
36 L. Yang, Q. X. Chen, Y. P. Wan, S. L. Gan, S. L. Li, C. S. Lee, Y. Jiang, H. T. Zhang and H. Y. Sun, *Chem. Commun.*, 2022, **58**, 9425–9428.
37 A. Silswal, A. Kanojiya and A. L. Koner, *Front. Chem.*, 2022, **10**, 840297.
38 A. Silswal, A. Pramanik and A. L. Koner, *J. Mater. Chem. B*, 2024, **12**, 489–499.
39 A. Silswal and A. L. Koner, *Chem. Commun.*, 2023, **59**, 1769–1772.
40 F. Jbilou, I.-N. Georgousopoulou, S. Marinkovic, S. Vouyiouka, C. D. Papaspyrides, B. Estrine, P. Dole, A. Cottaz and C. Joly, *Eur. Polym. J.*, 2016, **78**, 61–71.
41 P. Minei, G. Iasilli, G. Ruggeri, V. Mattoli and A. Pucci, *Chemosensors*, 2021, **9**, 3.
42 X. Y. Peng and Y. Yao, *Carbohydr. Polym.*, 2020, **250**, 116859.
43 G. Iasilli, F. Martini, P. Minei, G. Ruggeri and A. Pucci, *Faraday Discuss.*, 2017, **196**, 113–129.